ACCSCIENCE PUBLISHING

Gene & Protein in Disease

ORIGINAL RESEARCH ARTICLE

A novel signature identified by pyroptosis-related lncRNAs clusters predicts prognosis and tumor immune microenvironment for pediatric acute myeloid leukemia

Jie Lu, Xinyu Chang, Guowei Zheng, Xiting Cao, Zhenwei Wang, Hao Zhu, Shuaijie Gao, and Yuanlin Xi*

Department of Epidemiology and Biostatistics, College of Public Health, Zhengzhou University, Zhengzhou 450001, Henan, China

Abstract

Pyroptosis is a recently discovered programmed cell death that is involved in tumor formation, prognosis, and curative effect. Pyroptosis-related long non-coding ribonucleic acids (PR-lncRNAs) play key roles in tumorigenesis and tumor progression. However, the inherent relationship between PR-lncRNAs and the prognosis of pediatric acute myeloid leukemia (AML) remains unclear. For this reason, the association of PR-lncRNAs with the prognosis and tumor microenvironment features was analyzed using the Therapeutically Applicable Research to Generate Effective Treatment (TARGET) database. We classified three clusters based on PR-lncRNAs expressions and identified 841 differentially expressed PR-lncRNAs related to overall survival time. Seven key lncRNAs were then identified by least absolute shrinkage and selection operator (LASSO)-Cox and multivariate Cox. A signature based on these seven lncRNAs was also established, and the patients were separated into two groups according to their risk score. The high-risk group was characterized by poorer prognosis, lower expression of immune checkpoints, lower microsatellite instability or microsatellite stability (MSI-L/MSS), and lower drug sensitivity. The results demonstrated that PR-lncRNAs have a potential effect on the tumor immune microenvironment, clinicopathological features, and prognosis in pediatric AML. The nomogram and decision curve analysis suggested that the risk score is one of the most accurate of any other and provided a basis for the exploration of the immune microenvironment of the cell pyroptosis-associated subtypes in children with AML and the construction of a prognostic model with seven key PR-lncRNAs, which provides an approach to evaluate the prognosis of pediatric AML patients.

Keywords: Pediatric acute myeloid leukemia; Pyroptosis; Long non-coding RNAs; Prognostic signature; Tumor immune microenvironment

***Corresponding author:**
Yuanlin Xi
(xyl@zzu.edu.cn)

Citation: Lu J, Chang X, Zheng G, *et al.*, 2023, A novel signature identified by pyroptosis-related lncRNAs clusters predicts prognosis and tumor immune microenvironment for pediatric acute myeloid leukemia. *Gene Protein Dis*, 2(1):230.
https://doi.org/10.36922/gpd.v2i1.230

Received: October 19, 2022
Accepted: November 22, 2022
Published Online: December 28, 2022

1. Introduction

Acute myeloid leukemia (AML) is a hematologic malignancy with morphological, immunophenotypic, germline, and somatic cytogenetic and genetic abnormalities. Pediatric AML is the second most common form of leukemia in children, with a mortality

rate of 20–40% and a relapse rate of 30%[1]. Although there have been improvements in the prognosis of pediatric AML patients as a result of the latest advances in areas such as molecular pathological diagnostic techniques, risk stratification, and targeted supportive care, the overall survival (OS) in 2021 remains below 70%[1-3]. As known to all, its clinical outcomes and genetic backgrounds are different in each age group[4]. To date, there are only a number of well-designed and systematic studies that focus on the molecular mechanisms of pediatric AML. More efforts are thus needed to identify potential biomarkers that can monitor the prognosis of pediatric AML patients, as well as provide more efficient therapeutic strategies.

Pyroptosis is a gasdermin-mediated programmed cell death (PCD) initiated by inflammasomes that are critical for immunity[5-7]. The previous research has found that pyroptosis causes the release of inflammatory mediators IL-1β and IL-18 and prolongs the exposure of cells to an inflammatory environment, which may add to the risk of tumorigenesis[8]. To date, many studies have reported that pyroptosis is crucial in tumor invasion, proliferation, and metastasis, and it can regulate AML progression[7]. Existing studies have found that dipeptidyl peptidase (DPP)8 and DPP9 (DPP8/9), which are tiny molecules inhibiting serine dipeptidases, are related to pyrolysis through their activation of pro-caspase-1 in human AML cell lines and primary AML samples, which, in turn, trigger cell lysis and death, known as pyroptosis, and inhibit human AML progression. This is thought to be a promising therapeutic strategy for AML[9]. Besides, due to the physical interaction between caspase-associated recruitment domain 8 (CARD8) and caspase-1, the production of caspase-1-dependent interleukin (IL)-1β is negatively regulated in THP-1 (a human-monocyte cell line derived from an AML patient); this is similar to TP92[10,11]. Taking these results together, the role pyroptosis plays in pediatric AML which cannot be overlooked.

Long non-coding RNAs (lncRNAs) are expressed transcripts that do not encode proteins that are more than 200 nt in length. They are involved in the onset and development of AML[12,13]. Besides, it has been found that lncRNAs play crucial roles in humorous cellular processes, including pyroptosis. LncRNAs can regulate the expression of proteins related to the pyroptosis signaling pathway indirectly through miRNAs[14]. This kind of modulation exists in the pathological process of tumorigenesis as well. However, there is little research on pyroptosis-related lncRNAs (PR-lncRNAs) in pediatric AML. In addition, PR-lncRNAs' role in the prognosis of pediatric AML patients and its biological mechanism remain unclear. Furthermore, current evidence has suggested a link between pyroptosis and tumor microenvironment (TME), which is a dynamic network that includes tumor cells, immune cells, and stromal cells[15]. We hypothesize that PR-lncRNAs may affect progression of pediatric AML and the prognosis of these patients by interacting with the immune microenvironment. In this study, based on the Therapeutically Applicable Research to Generate Effective Treatment (TARGET) database, the relationship between PR-lncRNAs and the prognosis of pediatric AML patients was investigated; an evaluation of the predictive ability of the prognostic signature constructed by seven significant PR-lncRNAs was performed; and an exploration of whether PR-lncRNAs have an impact on the molecular microenvironment in pediatric AML was also carried out.

2. Materials and methods

2.1. Data acquisition

The gene expression and clinical data of 1474 pediatric AML samples were retrieved from the TARGET database up to March 1, 2022 (https://ocg.cancer.gov/programs/target). After excluding samples with incomplete clinical data, replications, and normal samples, 1300 pediatric AML samples were included for subsequent analyses.

2.2. Identification of pyroptosis-related lncRNAs and consensus clustering analyses

The lncRNA annotation file from the GENCODE website (GRCh38) (https://www.gencodegenes.org/human/) was used to distinguish lncRNAs and protein-coding genes. Meanwhile, 52 PR-lncRNAs were obtained from a website (http://www.broad.mit.edu/gsea/msigdb/) and relevant studies, as shown in Table S1. Pearson product-moment correlation coefficient was employed to distinguish PR-lncRNAs with $|\text{Pearson R}| > 0.4$ and $P < 0.001$. Univariate Cox regression analysis (Uni-Cox) was implemented to screen prognosis and pyroptosis-related lncRNAs (PPR-lncRNAs), while taking overall survival (OS) as the endpoint. The pediatric AML samples were divided into different clusters according to PPR-lncRNAs expressions by R package "ConsensusClusterPlus."

2.3. Relationship and differences among different clusters

The difference in OS among the clusters was determined using Kaplan–Meier (K-M) curves and a log-rank test. Kyoto Encyclopedia of Genes and Genomes (KEGG) gene sets in Gene Set Enrichment Analysis (GSEA) (version 4.2.3) were applied to three clusters to explore the distinctions of enriched pathways. The Estimation of STromal and Immune cells in MAlignant Tumor tissues using Expression data (ESTIMATE) scoring of the tumor microenvironment and the relative proportions of 22 immune cell infiltrations were calculated using

ESTIMATE and cell type identification by estimating relative subsets of RNA transcription (CIBERSORT) algorithms[16], respectively. Furthermore, the correlations among different subtypes in the expression of five immune checkpoints, including programmed cell death protein 1 (PD-1), programmed cell death-ligand 1 (PD-L1)[17], cytotoxic T-lymphocyte-associated protein 4 (CTLA-4)[18], lymphocyte-activation gene 3 (LAG3)[19], and hepatitis A virus cellular receptor 2 (HAVCR2/TIM-3)[20] pathways, which are implicated in tumor immune evasion and derived from previous studies, were analyzed.

2.4. Differentially expressed lncRNAs recognition and prognosis and pyroptosis-related lncRNAs signature construction

Differently expressed lncRNAs (DE-lncRNAs) within the three clusters were identified by the "limma" package in R according to the following criteria: log2FC ≥ 1 and adjusted $P < 0.001$. Uni-Cox was used to filter for DE-lncRNAs according to prognosis. These lncRNAs were then used to form PPR-lncRNAs signaling to predict the prognosis of pediatric AML patients. First, 1300 pediatric AML samples were randomly sorted into training and testing sets at a ratio of 7:3. LASSO-Cox ten-fold cross-validation and multivariate Cox regression analysis (multi-Cox) were used to establish the PPR-lncRNAs signature in the training set. The formula for calculating the risk score is shown below:

$$\text{riskscore} = \sum_{i=1}^{n} \text{coef}_i * x_i$$

Where coef_i represents the coefficients and x_i represents the count of PPR-lncRNAs expressions. Based on the calculation of the risk score, the pediatric AML samples in the training and testing sets were divided into high- and low-risk groups based on the median risk score of the training set.

2.5. Validation of the signature

K-M curves, ESTIMATE and CIBERSORT scores, and immune checkpoint expression were used to assess the differences between the two groups. Moreover, time-dependent receiver operating characteristic (ROC) curves were used to assess the predictive ability of the prognostic signature for OS.

Subgroup analyses of the selected clinical characteristics (age, gender, race, bone marrow leukemic blast percentage [BM], peripheral blasts [PB], white blood cell at diagnosis [WB], and French-American-British [FAB] category) were performed. Chi-squared (χ^2) test was performed to evaluate the distribution among subtypes, risk scores, and clinical variables. Independent factors in the prognosis of pediatric AML patients were identified through uni-Cox and multi-Cox analyses. Stratification analyses were performed to determine the stability of each clinical factor.

The semi-inhibitory concentration (IC50) values of chemotherapeutic drugs that are generally used to treat AML were estimated by the "prophetic" package in R[21]. Besides, the "PreMSIm" package was used to predict the microsatellite instability (MSI) state in both high- and low-risk groups based on the 15 genes expression.

Furthermore, Gene Ontology (GO) and KEGG enrichment analyses were performed to determine the function of the differentially expressed genes (DEGs) between the two groups. The DEGs were screened with $|\log2FC| \geq 1$ and false discovery rate (FDR) < 0.05.

2.6. Establishments of a nomogram and a decision curve

Combining the signature with clinical factors, a nomogram was constructed, integrating the prognostic signature using the "rms" package in R, to predict the 1-, 3-, and 5-year survival probability of pediatric AML patients. In addition, a decision curve analysis (DCA) was used to calculate the net benefit of each factor on the survival of pediatric AML patients at 1, 3, and 5 years.

2.7. Statistical analysis

In our study, statistical analyses were performed using R software (version 4.1.2). If not specifically stated, all results were regarded as statistically significant when $P < 0.05$.

3. Results

Figure 1. Flow chart of 1300 samples with complete clinical data from the TARGET database. Following Pearson correlation analysis and uni-Cox, 841 prognosis, and pyroptosis-related lncRNAs were obtained. Three clusters were classified by consensus clustering according to pyroptosis-related lncRNAs. Based on these three clusters, prognostic signature construction and immune difference exploration were performed.

Table 1 shows the characteristics of 1300 pediatric AML patients from the TARGET database. All 1300 AML patients with their OS information were used for prognostic model construction. From the expression matrix of 11,535 lncRNAs and 52 pyroptosis-related genes (PRGs), we identified 1792 lncRNAs as significant pyroptosis-associated genes by Pearson (Table S1). Three clusters were classified by unsupervised consensus clustering analysis and uni-Cox based on PR-lncRNAs (Figure 2A-C). The age, gender, and race components did not show any statistical difference ($P > 0.05$). Three-

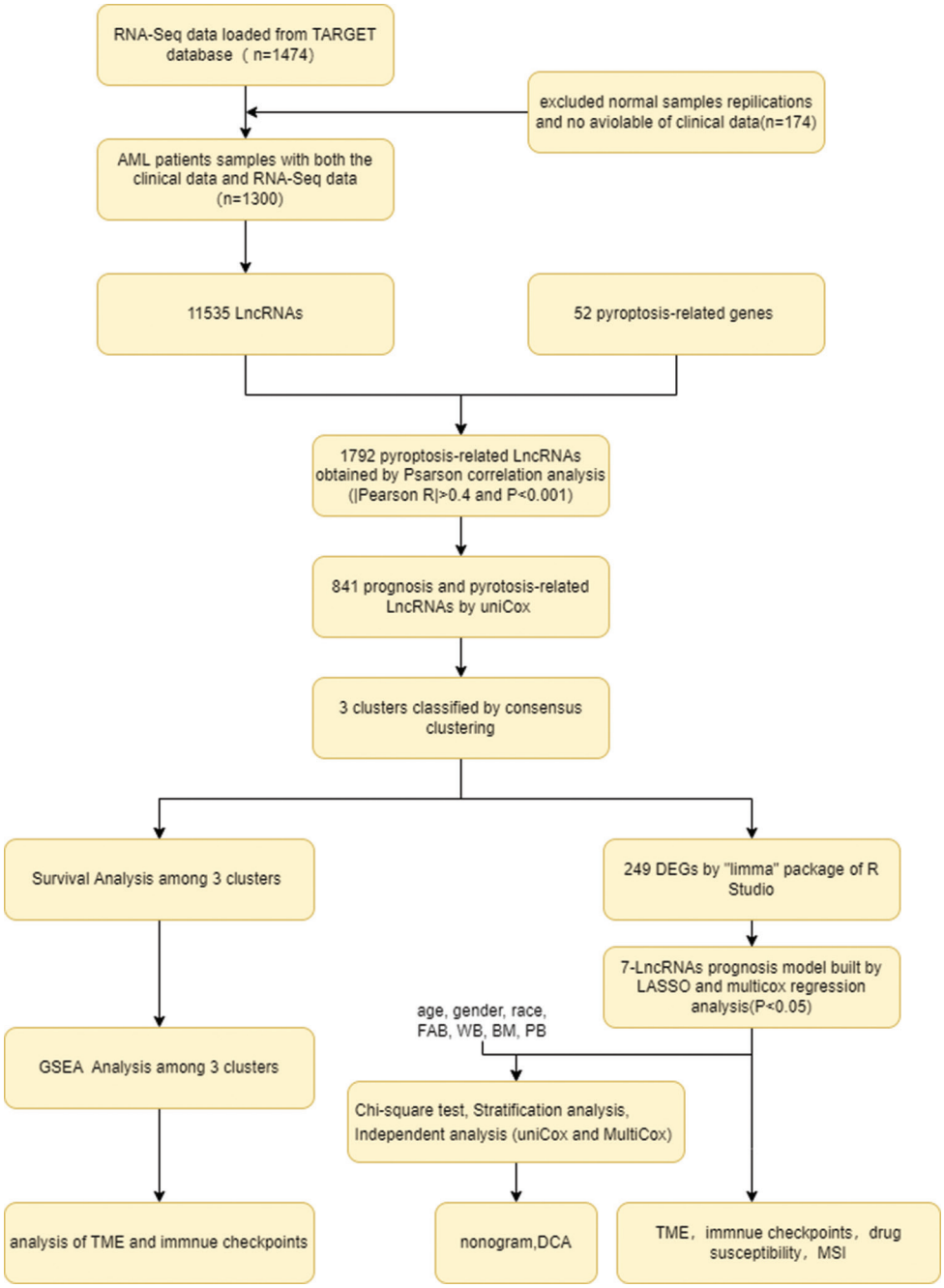

Figure 1. Flow chart of 1300 samples with complete clinical data extracted from the TARGET database.

dimensional (3D) PCA (principal component analysis) showed that the patients can be separated into three clusters by PPR-lncRNAs expressions (Figure 2D).

3.1. Correlations and differences among the three clusters

Table 1 shows that the laboratory indices (WB, BM, and PB) among the three clusters were significantly different. The K–M curve and log-rank test result of clusters 1–3 reflected statistical differences in terms of prognosis (Figure 2E) (P = 0.048), with cluster 3 having a better prognosis than cluster 1 (P = 0.020). Unexpectedly, the curves of clusters 1 and 2, and clusters 2 and 3 did not show significant distinctiveness; hence, the difference in survival from these two comparisons could not be identified. The result of GSEA among the three clusters (Tables S3 and S4) showed that genes in cluster 1 and cluster 2 were enriched in disease and metabolic pathways, and as expected, those

Table 1. Baseline characteristics of 1300 pediatric acute myeloid leukemia patients.

Characteristic	Cluster1 (n = 121)	Cluster2 (n = 137)	Cluster3 (n = 1,042)	Total (n = 1,300)	*P*
Gender					
Male	66 (5.08)	77 (5.92)	538 (41.38)	681 (52.38)	0.531
Female	55 (4.23)	60 (4.62)	504 (38.77)	619 (47.62)	
Age					
<3	21 (1.62)	39 (3.00)	253 (19.46)	462 (35.54)	0.19
3~6	14 (1.08)	12 (0.92)	124 (9.54)	150 (11.54)	
6~14	50 (3.85)	47 (3.62)	322 (24.77)	419 (33.23)	
≥14	36 (2.77)	40 (3.08)	343 (26.38)	419 (33.23)	
Race					
White	84 (6.46)	102 (7.85)	752 (57.85)	938 (72.15)	0.663
Not white	25 (1.92)	28 (2.15)	184 (14.15)	237 (18.23)	
Unknown	12 (0.92)	7 (0.54)	106 (8.15)	125 (9.62)	
WB	81.35±93.70	76.63±86.19	62.77±95.76	65.96±94.76	<0.01
<50	64 (4.92)	71 (5.46)	697 (53.62)	831 (63.92)	
≥31	58 (4.46)	66 (5.08)	344 (26.46)	468 (36.00)	
Unknown	0 (0.00)	0 (0.00)	1 (0.08)	1 (0.08)	
BM	70.15±50.70	71.62±19.54	62.19±25.51	63.97±24.74	<0.01
<70	51 (3.92)	45 (3.46)	491 (37.77)	587 (45.15)	
≥87	66 (5.08)	86 (6.62)	472 (36.31)	624 (48)	
Unknown	4 (0.31)	6 (0.46)	79 (6.08)	89 (6.85)	
PB (%)	59.07±28.14	57.54±27.33	41.46±31.68	44.83±31.63	<0.01
<70	71 (5.46)	83 (6.38)	756 (58.15)	910 (70)	
≥10	49 (3.77)	54 (4.15)	268 (20.62)	371 (28.54)	
Unknown	1 (0.08)	0 (0.00)	18 (1.38)	19 (1.46)	
FAB (%)					
M0	4 (0.31)	4 (0.31)	0 (0.00)	8 (0.62)	<0.01
M1	18 (1.38)	15 (1.15)	0 (0.00)	33 (2.54)	
M2	30 (2.31)	33 (2.54)	0 (0.00)	63 (4.85)	
M3	0 (0.00)	0 (0.00)	0 (0.00)	0 (0.00)	
M4	24 (1.85)	36 (2.77)	0 (0.00)	60 (4.62)	
M5	23 (1.77)	25 (1.92)	2 (0.15)	50 (3.85)	
M6	1 (0.08)	1 (0.08)	1 (0.08)	3 (0.23)	
M7	2 (0.15)	6 (0.46)	2 (0.15)	10 (0.77)	
Unknown	19 (1.46)	17 (1.31)	1,037 (79.77)	1,073 (82.54)	

BM: Bone marrow leukemic blast percentage, FAB: French-American-British category, M1: Acute myeloblastic leukemia with minimal maturation; M2: Acute myeloblastic leukemia with maturation, M3: Acute promyelocytic leukemia, M4: Acute myelomonocytic leukemia, M5: Acute monocytic leukemia, M6: Acute erythroid leukemia, M7: Acute megakaryoblastic leukemia, PB: Peripheral blasts, WB: White blood cell at diagnosis

in cluster 3 were enriched in main immune-associated pathways, such as B-cell and T-cell receptor signaling pathway, Fc epsilon RI, P53, and JAK-STAT signaling pathway, as well as Toll-like and NOD-like receptor signaling and apoptosis (Figure S1).

The interquartile range of age was 9.73 (3.29, 15.08). The minimum age was 0.01, and the maximum age was 29.59.

Seven variables were taken as covariates, and all covariates were taken as categorical variables.

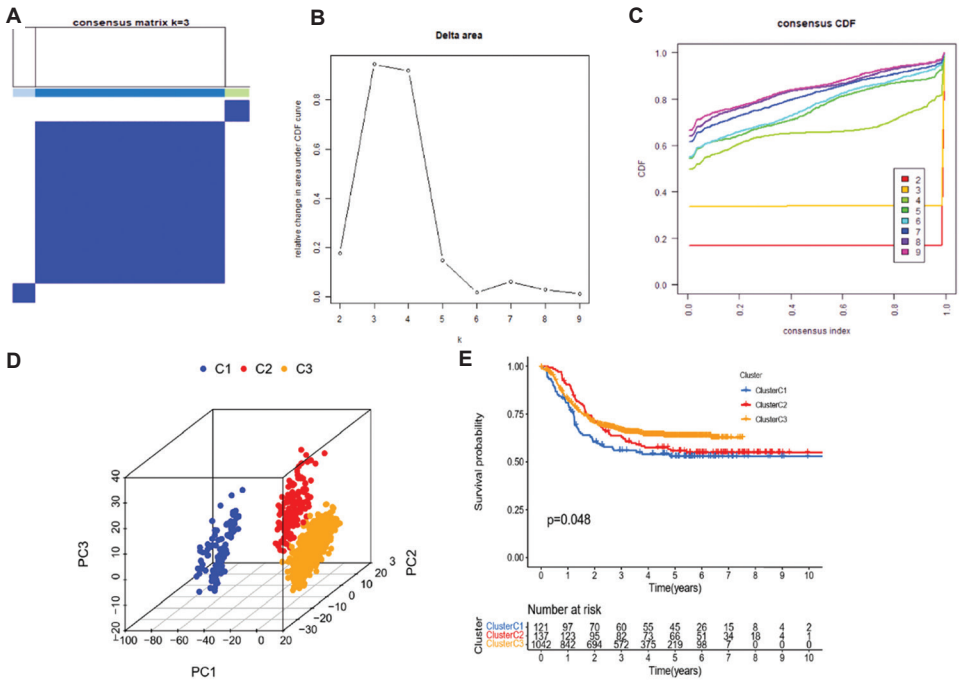

Figure 2. Consensus clustering of 841 prognosis and pyroptosis-related lncRNAs. (A) Consensus clustering matrix for k = 3. (B) Relative change in area under the cumulative distribution function (CDF) curve in pediatric AML. The cluster (k) selection criteria are the CDF changes steadily and its value is not very small. (C) CDF for pediatric AML. Choose the curve with a lower CDF decline slope among the curves with horizontal coordinates ranging from 0.1 to 0.9. (D) Three-dimensional principal component analysis of the three clusters. (E) Kaplan–Meier curves of the overall survival (OS) of pediatric AML patients in clusters 1–3.

The results of ESTIMATE were compared among the three clusters, and the scores were all remarkably lower in cluster 3 but higher in cluster 2 (Figure 3A–C). The tumor purity of three clusters is shown in Figure 3D. Moreover the proportion of each immune cell was compared among the three clusters, as shown in Figure 4A–C. We found that 7, 13, and 9 tumor-infiltrating immunocytes were statistically different between clusters 1 and 2, 2 and 3, as well as 1 and 3, respectively. Resting memory CD4 T-cells, follicular helper T-cells, resting NK cells, activated NK cells, resting (M0) macrophages, activated mast cells, eosinophils, and neutrophils were all significantly higher in cluster 3 (Figure S2). We also compared five important immune checkpoints (Figures 3E–I): PD-1, LAG-3, CTLA-4, PD-L1, and TIM-3. Except for TIM-3, all checkpoints had lower expressions in cluster 3.

3.2. Construction of the prognostic signature

A total of 249 DE-lncRNAs were screened out from the clusters by the "limma" package (shown in Figure 4A) ($log2|FC| > 1, P < 0.001$). Through uni-Cox, 122 prognosis-related DE-lncRNAs were selected with $P < 0.05$ as the threshold (Table S2), and 1300 pediatric AML samples were randomly divided into a training set (n = 912) and a testing set (n = 388) at a ratio of 7:3. Subsequently, LASSO-Cox regression and ten-fold cross-validation were used to reduce the complexity of the candidate lncRNAs, and 21 target lncRNAs were obtained. Seven lncRNAs (Table 2), related to six PRGs (Table S5), were obtained using multi-Cox and included in the final prediction model. Risk score = (-0.103223332 * *TRAF3IP2-AS1* – 0.013058209 * *AL157871.6* – 0.001632721 * *SNHG29* + 0.060510168 * *ASB16-AS1* + 0.083744921 * *AC007216.3* + 0.224003784 * *AP001318.1* + 0.230400789 * *AC127496.5*). The samples were separated into high- and low-risk groups according to the median risk score of the training set. The mortality rates of the samples in the two groups were significantly different based on a visual display of the risk score through ranked dot and scatter plots (Figure 4D–I). The K–M curves showed that the mortality rate of patients in the high-risk group was higher than that in the low-risk group (Figure 5A–C). The ROC curves were used to assess the predictive ability of the risk score for OS. The AUC (area under the ROC curve) was 0.663, 0.659, and 0.645 at 1, 3, and 5 years, respectively, in all groups; the AUC of the training set 1, 3, and 5 years is 0.676, 0.671, and 0.665 at 1, 3, and 5 years, respectively; the AUC of the testing set was 0.620, 0.642, and 0.601 at 1, 3, and 5 years, respectively (Figure 5D–F).

3.3. Validation of the prognosis and pyroptosis-related lncRNAs signature with clinical variables

Based on the clinical variables (gender, age, race, FAB category, WB, BM, and PB), Chi-squared (χ^2) test was

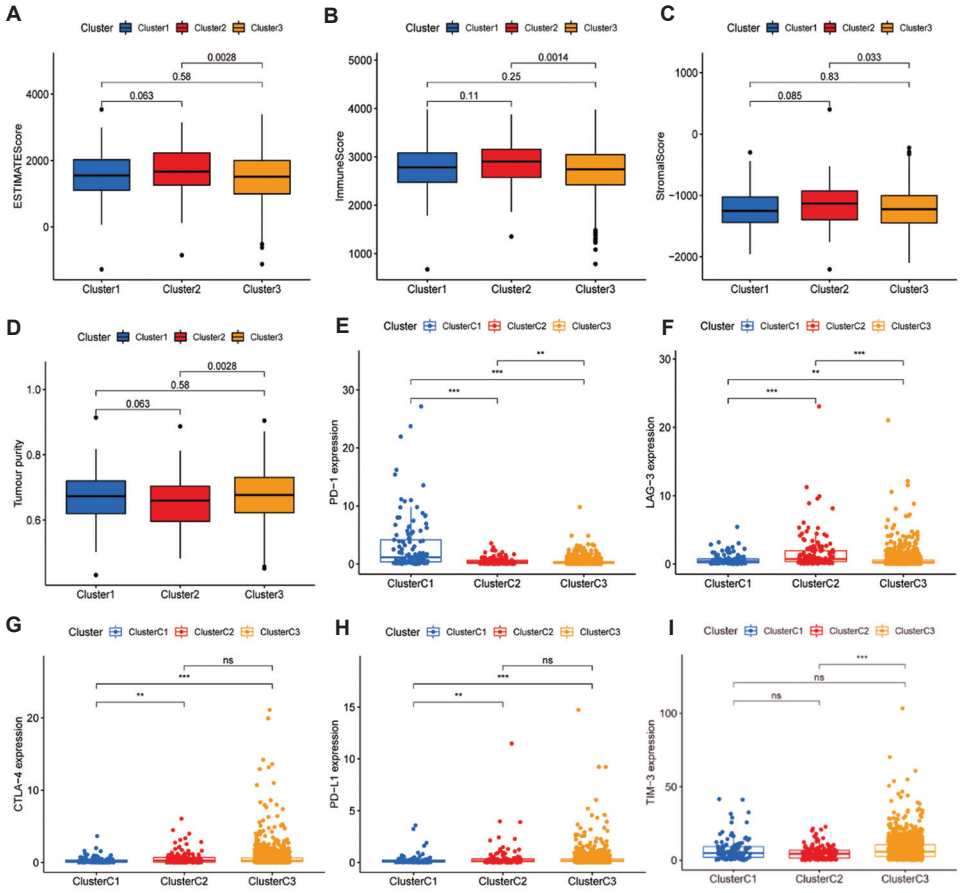

Figure 3. Immunological analysis. (A) Differences in ESTIMATE score among the three clusters. (B) Differences in immune score among the three clusters. (C) Differences in stromal score among the three clusters. (D) Differences in tumor purity among the three clusters. (E–I) Expression of five immune checkpoints in the three clusters: (E) PD-1; (F) LAG-3; (G) CTLA-4; (H) PD-L1; and (I) TIM-3.

performed to determine if there are differences in the baseline data between the two groups. The results showed statistical differences in age, BM, and FAB category. As observed in the heatmap shown in Figure 6, DE-lncRNAs were highly expressed in the high-risk group, especially in cluster 1, and age < 3 was more common with high risk (Figure 7A, C). As Figure 7B shown, the risk score was different in some FAB categories. Uni-Cox and multi-Cox were performed in combination with clinical characteristics and risk scores for prognostic markers to further explore independent prognostic factors (Figure 7D–E). Whether with uni-Cox or multi-Cox, the results showed that the prognostic signature might predict OS in pediatric AML patients independently. In addition, the stratified analyses performed to evaluate whether the prognostic signature retained its predictive ability in different subgroups, including age (< 3; ≥ 3 or < 6; ≥ 6 or < 14; and ≥ 14 years), race (white and others), gender (male and female), WB (< 50 and ≥ 50), PB (< 70 and ≥ 70), BM (70 and ≥ 70), and FAB (M1, M4, and M5), revealed notably lower OS in higher-risk patients compared to lower-risk patients (Figure S3).

3.4. Immune-related analysis

As shown in Figure 8A, the proportions of memory B-cells, plasma cells, naive CD4 T-cells, resting memory CD4 T-cells, resting mast cells, activated mast cells, and eosinophils were significantly lower in high-risk patients. Contrariwise, the proportions of naive B-cells and monocytes were significantly higher in high-risk patients. To identify the differences in tumor-infiltrating immune cells between the two groups, the stromal score, immune score, ESTIMATE score, and tumor purity were compared. As shown in the box chart (Figure 8B), the immune and ESTIMATE scores were significantly lower in the low-risk group; although tumor purity showed a different result, the tumor purity for both the groups was higher than 60. The expression of five important immune checkpoints was compared between the high- and low-risk groups. In the high-risk group, the expression of the checkpoints was higher except for TIM-3 (Figure 8C–G).

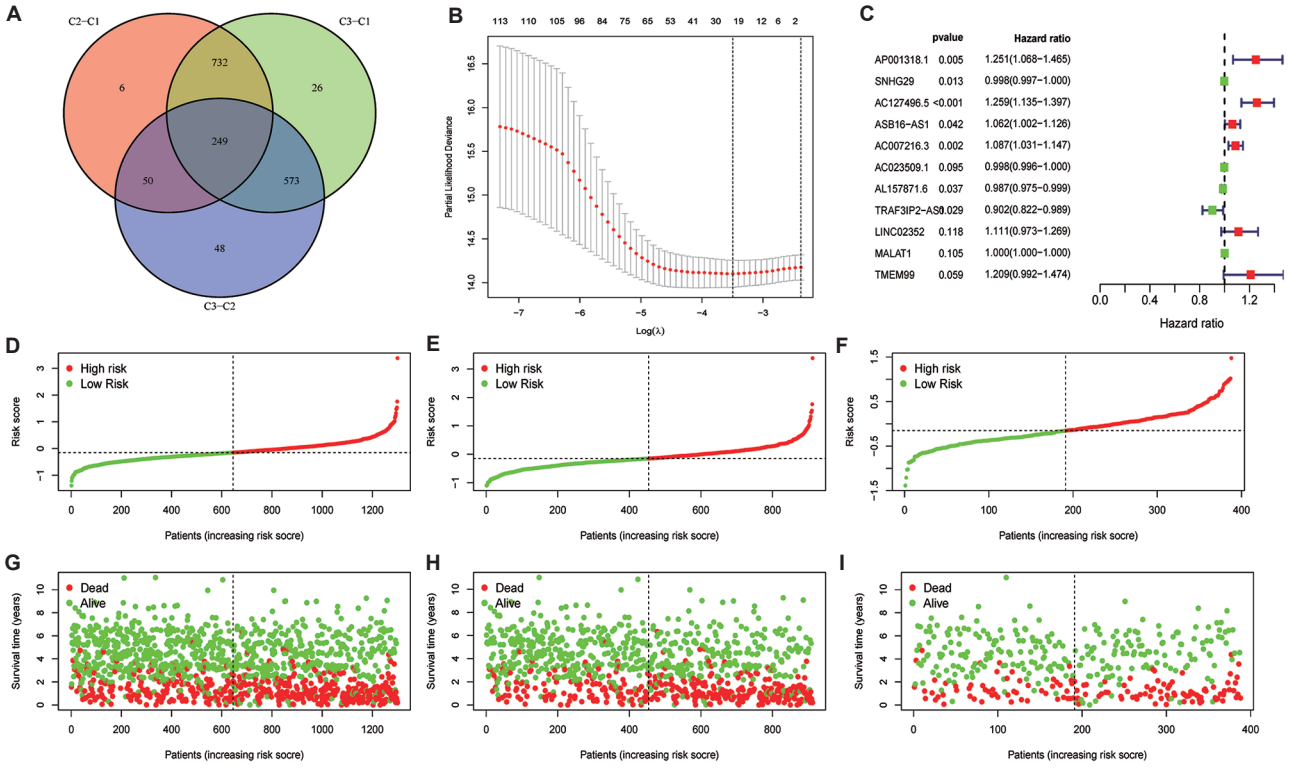

Figure 4. Construction of the prognostic signature of differentially expressed PR-lncRNAs in the training set. (A) Differentially expressed PR-lncRNAs among the three clusters. (B) Result of least absolute shrinkage and selection operator (LASSO) regression. (C) Multivariate Cox regression was performed. (D–I) Ranked dot and scatter plots showing the signature distribution and patient survival status: (D, G) in all sets; (E, H) in the training set; and (F, I) in the testing set.

Table 2. Seven lncRNAs obtained by multi-Cox regression.

LncRNA	Coef	HR	HR.95L	HR.95H	*P*
AP001318.1	0.224	1.251	1.068	1.465	0.0054
SNHG29	−0.002	0.998	0.997	1.000	0.0131
AC127496.5	0.230	1.259	1.135	1.397	0.0000
ASB16-AS1	0.061	1.062	1.002	1.126	0.0417
AC007216.3	0.084	1.087	1.031	1.147	0.0021
AL157871.6	−0.013	0.987	0.975	0.999	0.0373
TRAF3IP2-AS1	−0.103	0.902	0.822	0.989	0.0288

Coef: Coefficient, HR: Hazard ratio, HR.95L: Lower limit of the 95% confidence interval, HR.95H: Higher limit of the 95% confidence interval

3.5. Drug susceptibility analysis

Eight chemotherapy drugs that are commonly used to treat AML were selected to evaluate the sensitivities of the pediatric AML samples in both the groups to these drugs (Figure 9A–H). The results showed that the half maximal inhibitory concentration (IC50) values of the majority of these drugs, including axitinib, bleomycin, lenalidomide, midostaurin, nilotinib, and thapsigargin, were significantly lower in low-risk patients. However, we were unable to demonstrate a similar difference with cytarabine.

3.6. Relationship between risk score and microsatellite instability

MSI is strongly associated with the risk score. As shown in Figure 9I–J, the low-risk group had a high proportion of MSI-H (high microsatellite instability) at 44%, and the average risk score of the patients in the MSI-H group was significantly higher than that in the MSI-L/MSS (low microsatellite instability or microsatellite stability) group ($P < 0.001$).

3.7. Discovery of molecular functions and pathways

To explore the biological functions and signaling pathways of the DEGs between the two groups, GO and KEGG were used. The DEGs between the two groups were identified according to the following criteria: log2| FC| > 1 and FDR < 0.05. The GO analysis that was performed included biological process (BP), molecular function (MF), and cell component (CC). The results of these three parts are presented in Figure 10A, indicating that tumor immunity

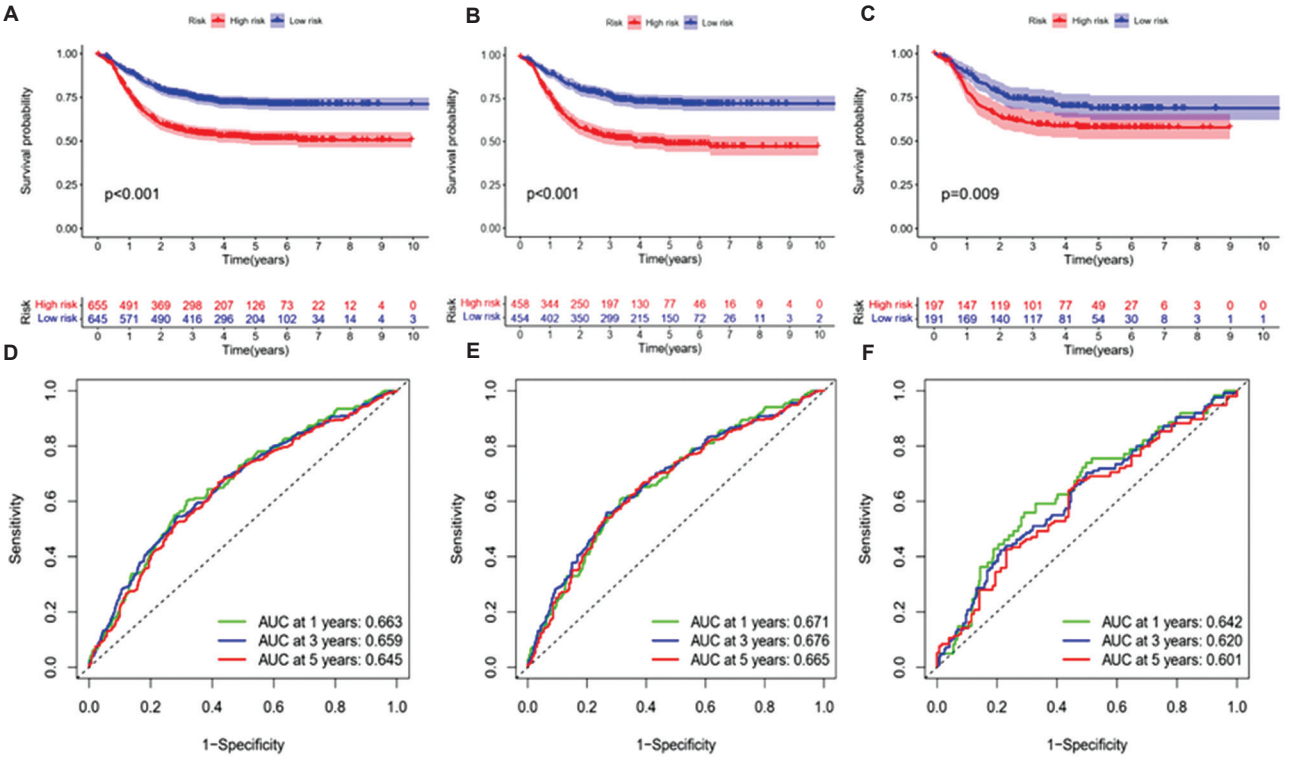

Figure 5. Identification of prognostic signature. (A–C) Kaplan–Meier curves showing that the low-risk group had superior overall survival than the high-risk group: (A) in all sets; (B) in the training set; and (C) in the testing set. (D–F) Area under ROC curves at 1, 3, and 5 years: (D) in all sets; (E) in the training set; and (F) in the testing set.

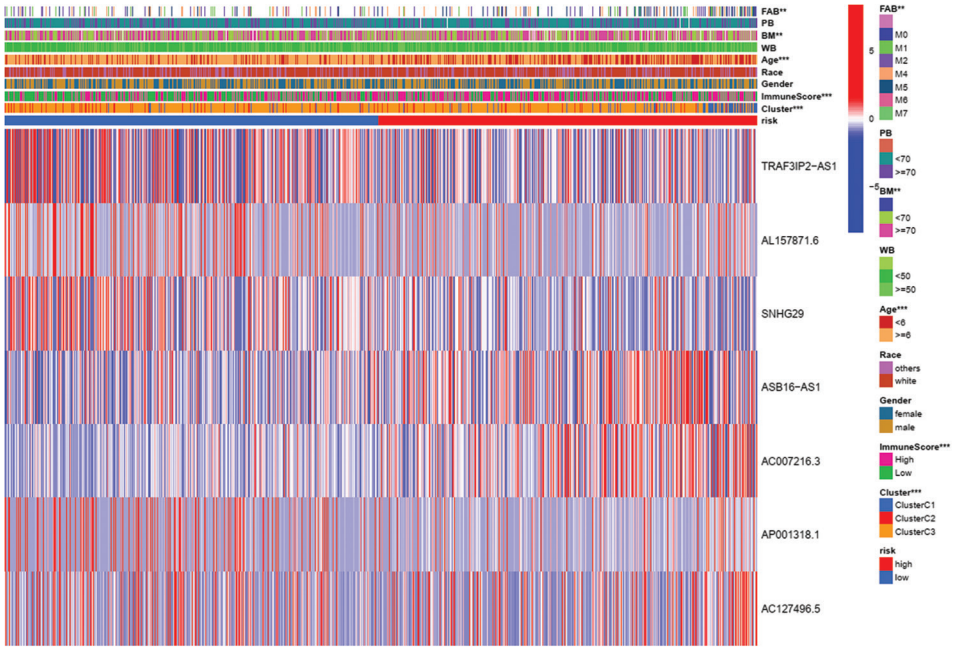

Figure 6. Heatmap. Abbreviations: BM: Bone marrow leukemic blast percentage (%); PB: Peripheral blasts (%); and WB: White blood cell at diagnosis.

and cell metabolism were the DEGs' main functions. KEGG analysis revealed that the enriched pathways were significantly related to the immune and hematopoietic system, including B-cell receptor signaling pathway,

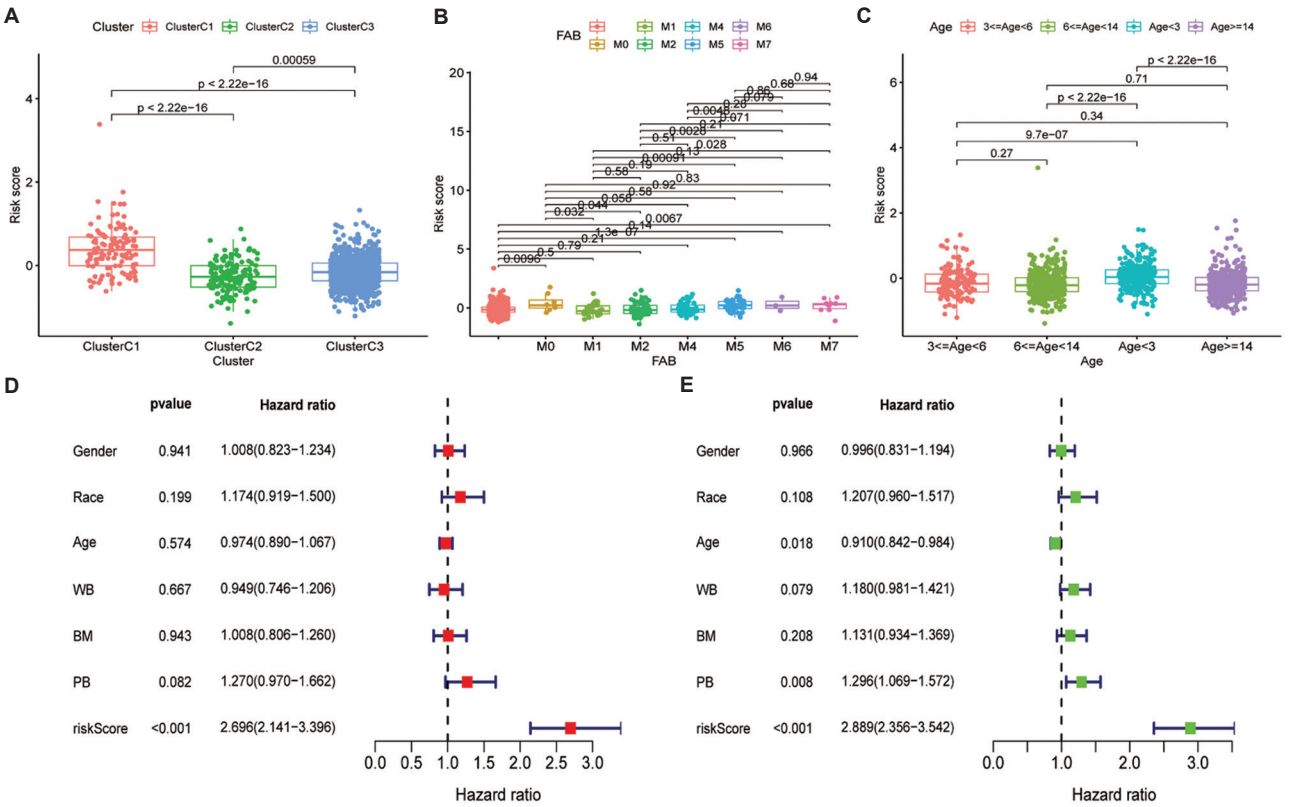

Figure 7. Relationship among the risk score, clinical features, clusters, and immune score in AML. (A–C) Risk score in different characteristics: (A) clusters; (B) FAB category; (C) age. (D) Results of multivariate Cox regression analysis. (E) Results of univariate Cox regression analysis.

human T-cell leukemia virus 1 infection, hematopoietic cell lineage, AML, and chronic myeloid leukemia (Figure 10B).

3.8. Establishments of a nomogram and a decision curve

To further enhance the clinical application value and provide a reliable predictive model for pediatric AML patients, the clinical parameters and risk scores were combined to build a nomogram (Figure 11A). The probability of survival in 1, 3, and 5 years can be calculated by a nomogram incorporating the score of seven PPR-lncRNAs and the clinicopathological parameters; its calibration curve is shown in Figure 11B. In addition, according to the 1-, 3-, and 5-year DCA curves shown in Figure 11C–E, the risk score was the optimal predictor of survival for pediatric AML patients.

4. Discussion

With the rapid advancements in bioinformatics, predicting the prognosis of pediatric AML patients by assessing the risk level of pediatric AML at the molecular level has become a reality. The regulatory mechanisms involved in the lncRNA-mediated regulation of AML suggest that lncRNAs can be used as potential molecular markers to predict the course and survival status of AML patients[22]. Pyroptosis plays a key role in tumorigenesis and tumor progression. At present, studies have found that PR-lncRNAs act as immunotherapy targets or diagnostic and predictive biomarkers for various cancer types, such as uterine corpus endometrial carcinoma, bladder cancer, colorectal cancer, and so on[23-26]. However, there is still a lack of systematic and in-depth studies on the relationship between lncRNAs and the prognosis of AML patients, especially pediatric AML patients.

In our study, we retrieved 1300 transcriptome data and the corresponding clinical data from the TARGET database and identified 841 PR-lncRNAs. We, then, classified three clusters according to the count of PR-lncRNAs expression. WB, BM, and PB were all remarkably lower in cluster 3. Pathways that genes enriched in better prognostic clusters (cluster 3) were mainly important immune-related signaling pathways, including B-cell and T-cell receptor signaling pathways, NOD-like and Toll-like receptor signaling pathways, and Fc epsilon RI signaling pathway, which were derived from GSEA. Comparing the better and the poorer prognostic clusters (cluster 3 and cluster 1), there were significantly different proportions in nine out of 22

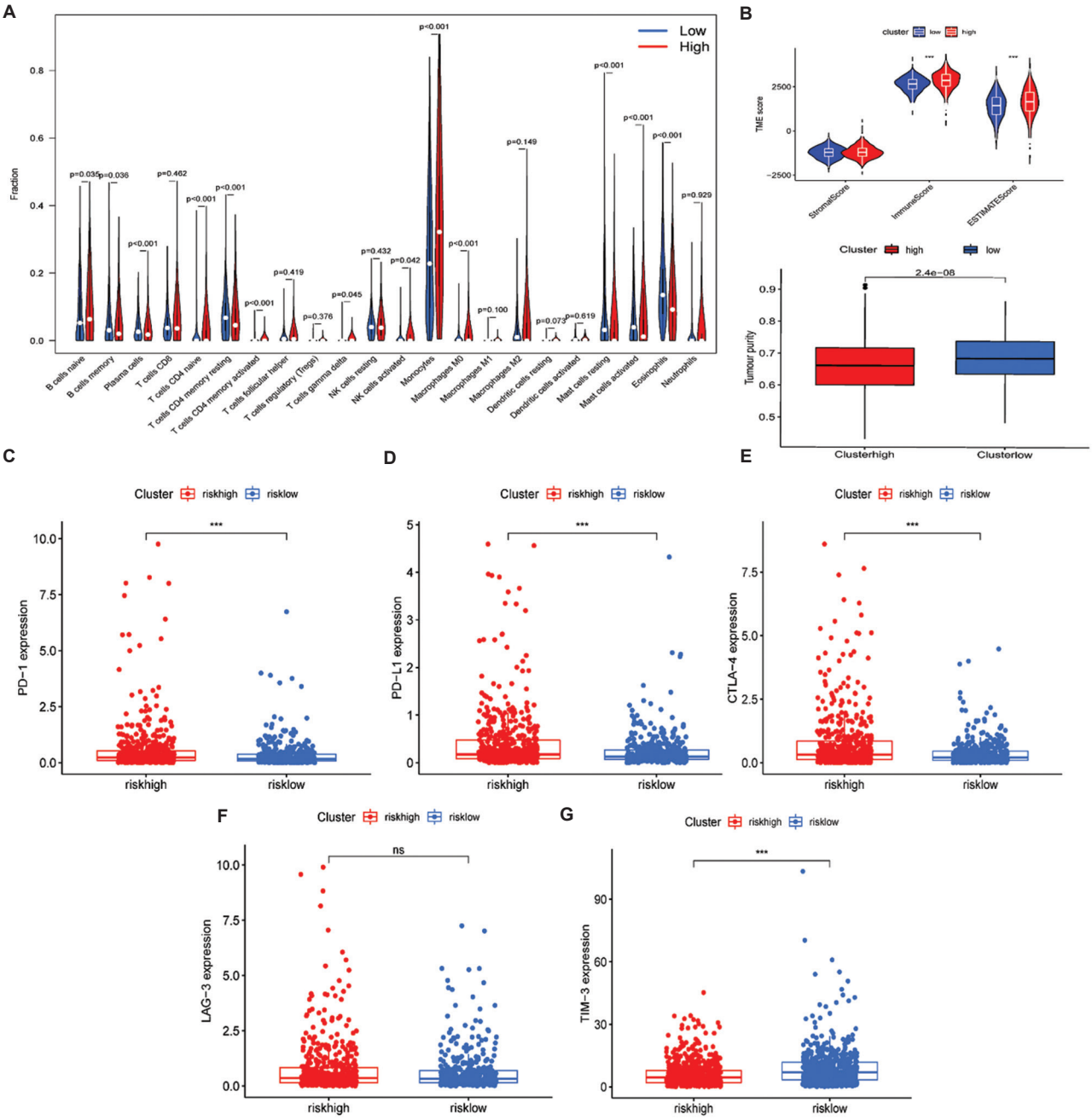

Figure 8. Immunological analysis between high- and low-risk groups. (A) Difference in the proportions of 22 immune cell types between the high- and low-risk groups. (B) Differences in ESTIMATE, stromal, and immune scores, and tumor purity between the two groups. (C–G) Expressions of five immune checkpoints between the two groups: (C) PD-1; (D) PD-L1; (E) CTLA-4; (F) LAG-3; and (G) TIM-3.

immune cell types. Although most of them were at a higher level in better prognosis patients, follicular helper T-cell, eosinophils, and activated NK cells showed the opposite. We classified cluster 3 as an immunoinflammatory subtype characterized by higher immune cell infiltration and better survival level. There were large proportions of monocytes in all populations, which may be related to the molecular types of acute monocytic leukemia (M4) and acute monocytic leukemia (M5). Interestingly, we found that there was no statistical difference between the three clusters based on the result of ESTIMATE. However, tumor purity was >60 for all, which is sufficient to ensure that the number of mutations read does not affect the biological interpretation of genome analysis[27].

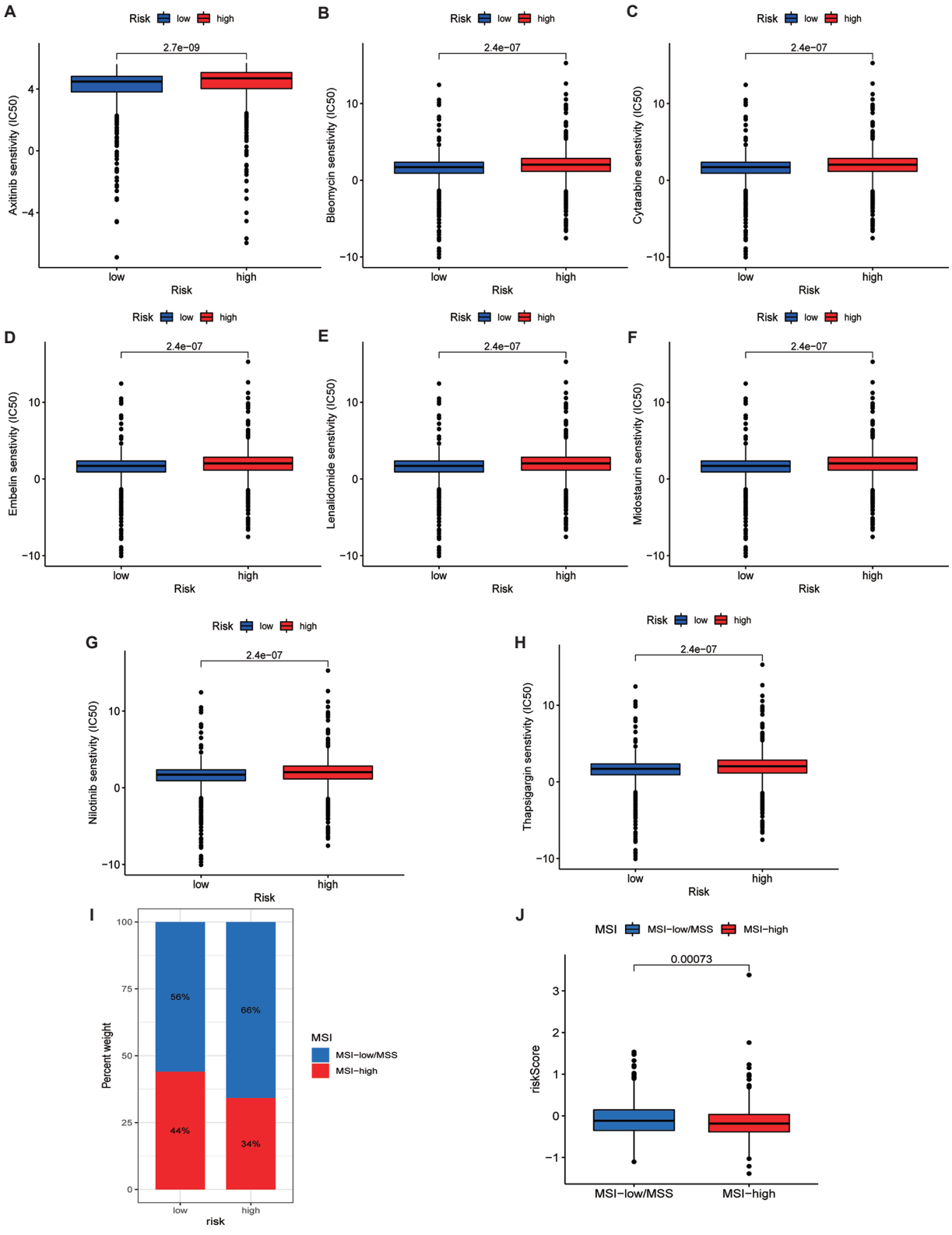

Figure 9. Results of drug sensitivity and microsatellite instability (MSI). (A–H) Relationships between signature and drug sensitivity. (I–J) Relationships between the signature and MSI.

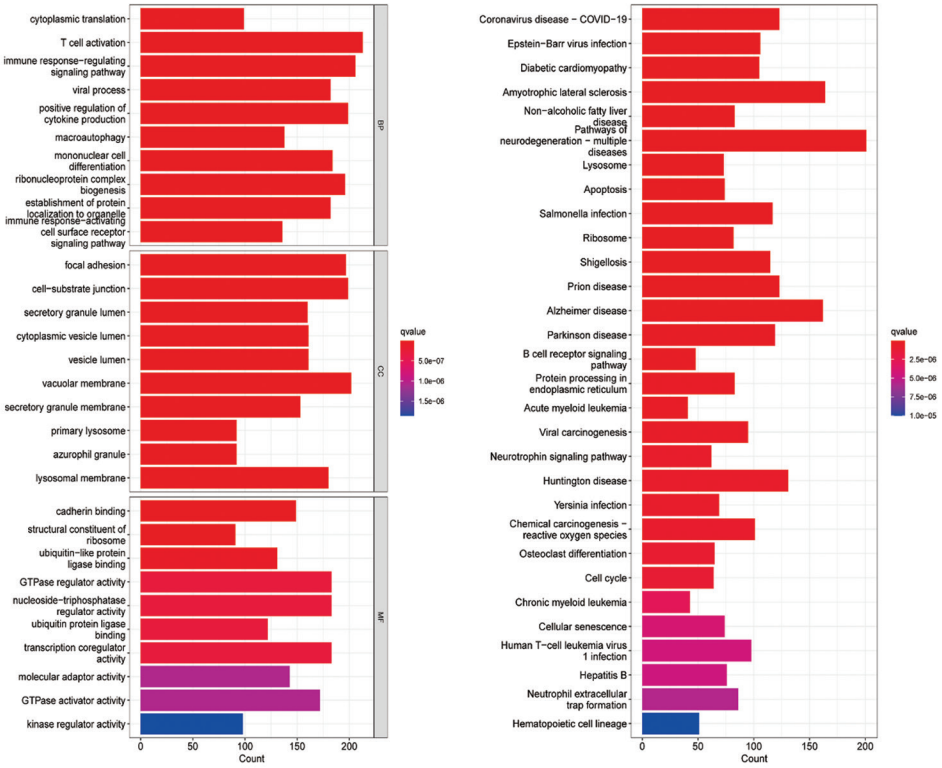

Figure 10. Representative results of Gene Ontology (GO) and Kyoto Encyclopedia of Genes and Genomes (KEGG) analyses. (A) GO and (B) KEGG.

Immune checkpoints are molecules that are expressed on immune cells and can regulate the immune process, thus playing an important role in immune effects[28]. The outcomes showed that there were significant differences in the expression of CTLA-4, PD-1, and PD-L1, which have been proven as essential immune checkpoints in pediatric AML, between clusters 1 and 3, with higher expressions in the poorer prognostic cluster (cluster 1); the results were similar to Jiang's study[29,30]. Interestingly, we also found that LAG3 had the same expression difference in these clusters.

Using LASSO-Cox and multi-Cox, we confirmed that seven out of 841 DE-lncRNAs are deserving of inclusion in the construction of a prognostic signature for predicting OS in pediatric AML, in which the 7 PPR-lncRNAs are *TRAF3IP2-AS1*, *AL157871.6*, *SNHG29*, *ASB16-AS1*, *AC007216.3*, *AP001318.1*, and *AC127496.5*. *TRAF3IP2-AS1*, which was lowly expressed in the high-risk group, has been found to play a key role in the etiopathogenesis of various autoimmune diseases by negatively regulating human IL-17 signaling through the downregulation of activator 1 (Act1) expression[31]. IL-17 is a pro-inflammatory cytokine that is secreted by activated CD4 T-cells, involved in inducing and mediating proinflammatory responses, and increasingly recognized as a risk factor of AML with poorer prognosis[32,33]. In other studies, *TRAF3IP2-AS1* has also been found to be related to N^6-methyladenosine and ferroptosis, affecting the prognosis and treatment of patients[34,35]. *SNHG29*, which was identified as a protective factor in our study, has been found in previous studies that it inhibits the ubiquitination degradation of yes-associated protein (YAP) by binding to it, thus promoting the expression of downstream target gene PD-L1 and subsequently anti-AML immunity[36,37]. Besides, in Han's study, they found that *SNHG29* has a role in carcinogenesis through the miR-223-3p/CTNND1 axis[38]. Besides, Li has found that *SNHG29* can indirectly affect the expression of *BAALC*, a gene upregulated in AML, by sponging miR-380-3p and negatively modulating miR-380-3p expression as a competing endogenous RNA (ceRNA)[39]. The expression of *ASB16-AS1* was positively associated with risk score in our study. In another study, *ASB16-AS1* affected more than ten immune-related signal pathways in multiple cancer types and played a key role in the recruitment and functional regulation of tumor-infiltrating immune cells[40]. In AML therapeutic area, NF-kappa B (NF-κB) pathway has been regarded as a target. In a study conducted by Bosman *et al.*, they discovered that the performance of transforming growth factor-β activated kinase 1 (TAK1) is related to the overexpression

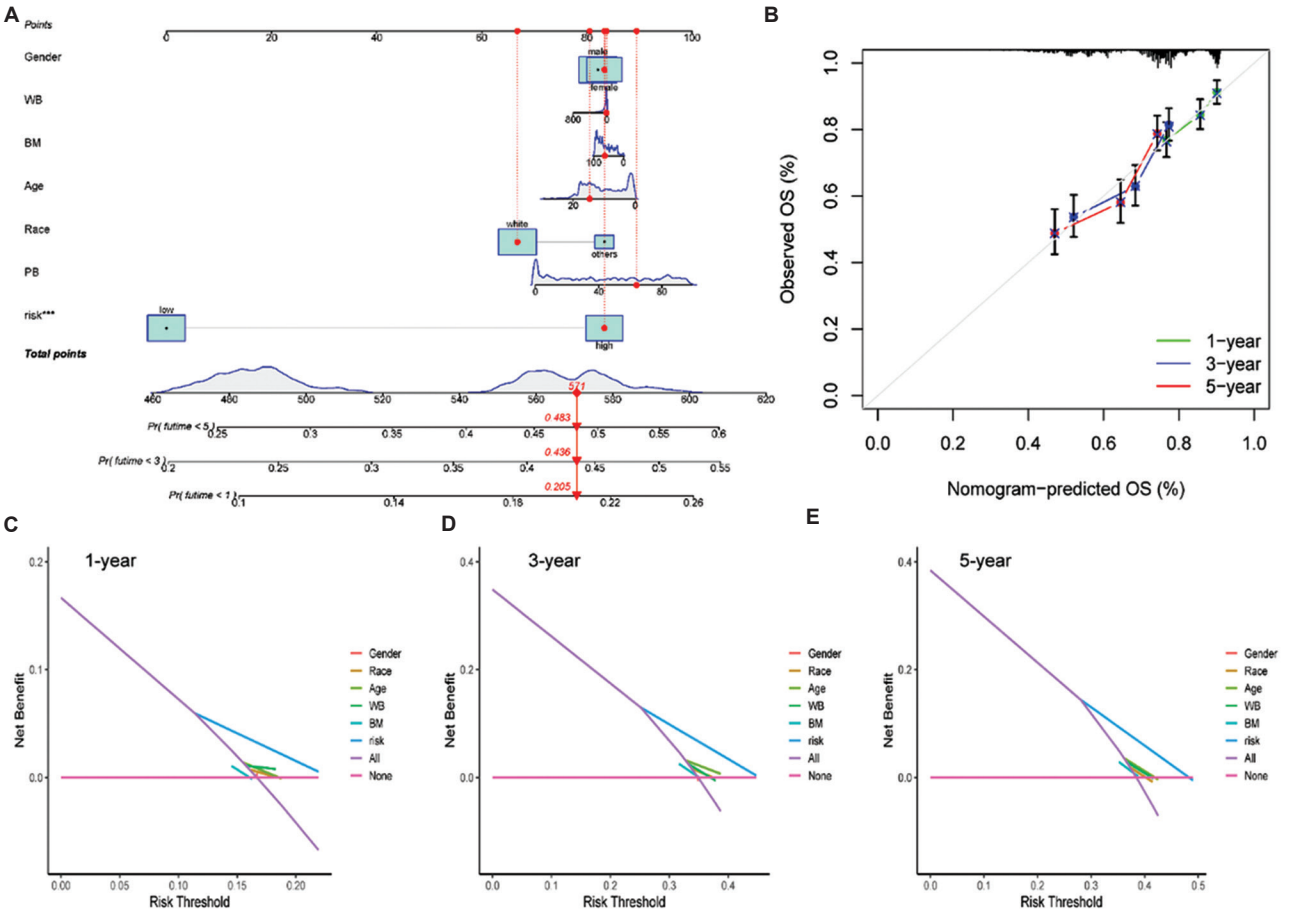

Figure 11. Decision curve and nomogram. (A) A nomogram with gender, race, BM, PB, WBC, age, FAB category, and risk score. (B) 1-, 3-, and 5-year calibration curves. (C–E) Decision curves at 1, 3, and 5 years. BM: Bone marrow leukemic blast percentage (%); PB: Peripheral blasts (%); WB: White blood cell at diagnosis.

and inhibition of NF-κB in AML CD34+cells[41]. In a study on gastric cancer, researchers have found that NF-κB can be stimulated by strengthening the expression of TRIM37 through *ASB16-AS1*[42]. *AC127496.5*, on the other hand, has been found to be one of the predictors of response to anti-PD-1 therapy for patients with cancer other than AML[43]. Unfortunately, we have not found the mechanism of the other three lncRNAs; thus, more research is needed to ascertain their potential roles.

Seven PR-lncRNAs were used to construct the pediatric AML prognostic signature, and the expression levels of those genes were calculated using risk scores. The AUC of the training set was 0.671, 0.676, and 0.665 at 1, 3, and 5 years, respectively. Similar results were obtained for the testing set in validating the model. The prediction model has a considerable effect on the survival prediction of pediatric AML patients, and the prognostic signature has a great predictive ability for these patients.

The low- and high-risk groups were separated according to the median risk score of the training set. Patients in the two groups showed noticeably distinct clinical characteristics, prognosis, TME, immune checkpoint expressions, MSI level, and drug susceptibility. The high-risk group was characterized by poorer prognosis, lower immune checkpoint expressions, MSI-L/MSS, and lower drug susceptibility. Interestingly, we found that one of the immune checkpoints, TIM-3, played a different role from others both in the risk groups and the three clusters. In the previous studies, researchers have found that TIM-3 may be different in AML and other leukemias; also, its representations may not be the same in different FAB categories. Studies have also found that TIM-3 played a different role in acute promyelocytic leukemia (M3) compared with other cases[44,45]. However, we were unable to find any association with M3 in our study. The molecular mechanisms involved in the different outcomes need to be further explored. As expected, the TME differed

in the presence of different PR-lncRNAs expressions. Recent studies have revealed that pyroptosis is a double-edged sword. On the one hand, pyroptosis-induced inflammation facilitates the generation and maintenance of an inflammatory microenvironment surrounding cancer cells, thus facilitating tumor development[46]. On the other hand, the acute activation of pyroptosis leads to the infiltration of various immune cells, thus repressing tumor development. Other studies have shown that many lncRNAs display a strong cell type-specific expression pattern in TME, especially in a variety of immune cell types[47]. Hence, PR-lncRNAs, combining the dual effects of pyroptosis and lncRNAs, may result in a different TME. Regrettably, with our study and previous research evidence, it is still impossible to conclude whether this effect is positive or negative. At the end of this study, we established a decision curve, inclusive of the risk score and clinical parameters. It showed that the risk score was the best predictor among various factors.

In this study, we built a prognostic signature and a nomogram based on seven PR-lncRNAs to predict the prognosis of pediatric AML patients and preliminarily explored the relationship between PR-lncRNAs and immune status, which have not been involved in the previous studies before. Nevertheless, there are still some gaps in our research. First, the data we used in our analysis were obtained from a public database; hence, the accuracy of the data cannot be verified. Second, our study did not include an external testing set; the prognostic signature was constructed and validated through the TARGET cohort. Last but not least, the potential relationship between the risk score and anticancer immunity needs to be further explored. Given the limitations above, the conclusions drawn from our study still require a higher degree of detailed experimental verification.

5. Conclusion

Pyroptosis and lncRNAs play a critical role in the progression of pediatric AML, the prognosis of these patients, and the alteration of TME. Our research validated an original PR-lncRNAs signature that is independently associated with OS. In addition, we identified the relevance of the immune microenvironment in influencing pediatric AML outcomes by analyzing the prognostic signature and immune profiles. The predictive value of the model needs to be examined by accurate clinical data. Moreover, the inherent mechanism by which PR-lncRNAs contribute to antitumor immunity remains to be revealed in future studies.

Acknowledgments

None.

Funding

This work was supported by the Natural Science Foundation of Henan Province, China (Grant No. 212300410402).

Conflict of interest

The authors declare no conflicts of interest.

Author contributions

Conceptualization: Xinyu Chang
Formal analysis: Xinyu Chang, Guowei Zheng, Xiting Cao, Zhenwei Wang, Hao Zhu, Shuaijie Gao
Writing – original draft: Xinyu Chang
Writing – review & editing: Jie Lu, Yuanlin Xi

Ethics approval and consent to participate

Not applicable.

Consent for publication

Not applicable.

Availability of data

The transcriptome data and clinical data of 1474 AML samples were retrieved from the TARGET database up to March 1, 2022 (https://ocg.cancer.gov/programs/target).

References

1. Quessada J, Cuccuini W, Saultier P, *et al*., 2021, Cytogenetics of pediatric acute myeloid leukemia: A review of the current knowledge (in eng). *Genes (Basel)*, 12(6): 924.

   https://doi.org/10.3390/genes12060924

2. Lejman M, Dziatkiewicz I, Jurek M, 2022, Straight to the point-the novel strategies to cure pediatric AML (in eng). *Int J Mol Sci*, 23(4): 1968.

   https://doi.org/10.3390/ijms23041968

3. Egan G, Chopra Y, Mourad S, *et al*., 2021, Treatment of acute myeloid leukemia in children: A practical perspective (in eng). *Pediatr Blood Cancer*, 68(7): e28979.

   https://doi.org/10.1002/pbc.28979

4. Kuwatsuka Y, Tomizawa D, Kihara R, *et al*., 2018, Prognostic value of genetic mutations in adolescent and young adults with acute myeloid leukemia (in eng). *Int J Hematol*, 107(2): 201–210.

   https://doi.org/10.1007/s12185-017-2340-z

5. Hsu SK, Li CY, Lin IL, *et al*., 2021, Inflammation-related pyroptosis, a novel programmed cell death pathway, and its crosstalk with immune therapy in cancer treatment (in eng). *Theranostics*, 11(18): 8813–8835.

   https://doi.org/10.7150/thno.62521

6. Li L, Jiang M, Qi L, *et al.*, 2021, Pyroptosis, a new bridge to tumor immunity (in eng). *Cancer Sci*, 112(10): 3979–3994.

   https://doi.org/10.1111/cas.15059

7. Fang Y, Tian S, Pan Y, *et al.*, 2020, Pyroptosis: A new frontier in cancer (in eng). *Biomed Pharmacother*, 121: 109595.

   https://doi.org/10.1016/j.biopha.2019.109595

8. Xia X, Wang X, Cheng Z, *et al.*, 2019, The role of pyroptosis in cancer: Pro-cancer or pro-"host"? (in eng). *Cell Death Dis*, 10(9): 650.

   https://doi.org/10.1038/s41419-019-1883-8

9. Johnson DC, Taabazuing CY, Okondo MC, *et al.*, 2018, DPP8/DPP9 inhibitor-induced pyroptosis for treatment of acute myeloid leukemia (in eng). *Nat Med*, 24(8): 1151–1156.

   https://doi.org/10.1038/s41591-018-0082-y

10. Razmara M, Srinivasula SM, Wang L, *et al.*, 2002, CARD-8 protein, a new CARD family member that regulates caspase-1 activation and apoptosis (in eng). *J Biol Chem*, 277(16): 13952–13958.

    https://doi.org/10.1074/jbc.M107811200

11. Luo X, Zhang X, Gan L, *et al.*, 2018, The outer membrane protein Tp92 of *Treponema pallidum* induces human mononuclear cell death and IL-8 secretion (in eng). *J Cell Mol Med*, 22(12): 6039–6054.

    https://doi.org/10.1111/jcmm.13879

12. Bhan A, Soleimani M, Mandal SS, 2017, Long noncoding RNA and cancer: A new paradigm (in eng). *Cancer Res*, 77(15): 3965–3981.

    https://doi.org/10.1158/0008-5472.Can-16-2634

13. Bridges MC, Daulagala AC, Kourtidis A, 2021, LNCcation: lncRNA localization and function (in eng). *J Cell Biol*, 220(2): e202009045.

    https://doi.org/10.1083/jcb.202009045

14. He D, Zheng J, Hu J, *et al.*, 2020, Long non-coding RNAs and pyroptosis (in eng). *Clin Chim Acta*, 504: 201–208.

    https://doi.org/10.1016/j.cca.2019.11.035

15. Weber CE, Kuo PC, 2012, The tumor microenvironment (in eng). *Surg Oncol*, 21(3): 172–177.

    https://doi.org/10.1016/j.suronc.2011.09.001

16. Newman AM, Liu CL, Green MR, *et al.*, 2015, Robust enumeration of cell subsets from tissue expression profiles (in eng). *Nat Methods*, 12(5): 453–457.

    https://doi.org/10.1038/nmeth.3337

17. Ohaegbulam KC, Assal A, Lazar-Molnar E, *et al.*, 2015, Human cancer immunotherapy with antibodies to the PD-1 and PD-L1 pathway (in eng). *Trends Mol Med*, 21(1): 24–33.

    https://doi.org/10.1016/j.molmed.2014.10.009

18. Rowshanravan B, Halliday N, Sansom DM, 2018, CTLA-4: A moving target in immunotherapy (in eng). *Blood*, 131(1): 58–67.

    https://doi.org/10.1182/blood-2017-06-741033

19. Maruhashi T, Sugiura D, Okazaki IM, *et al.*, 2020, LAG-3: From molecular functions to clinical applications (in eng). *J Immunother Cancer*, 8(2): e001014.

    https://doi.org/10.1136/jitc-2020-001014

20. Zang K, Hui L, Wang M, *et al.*, 2021, TIM-3 as a prognostic marker and a potential immunotherapy target in human malignant tumors: A meta-analysis and bioinformatics validation (in eng). *Front Oncol*, 11: 579351.

    https://doi.org/10.3389/fonc.2021.579351

21. Li L, Feng Q, Wang X, 2020, PreMSIm: An R package for predicting microsatellite instability from the expression profiling of a gene panel in cancer (in eng). *Comput Struct Biotechnol J*, 18: 668–675.

    https://doi.org/10.1016/j.csbj.2020.03.007

22. Garzon R, Volinia S, Papaioannou D, *et al.*, 2014, Expression and prognostic impact of lncRNAs in acute myeloid leukemia (in eng). *Proc Natl Acad Sci U S A*, 111(52): 18679–18684.

    https://doi.org/10.1073/pnas.1422050112

23. Liu J, Geng R, Ni S, *et al.*, 2022, Pyroptosis-related lncRNAs are potential biomarkers for predicting prognoses and immune responses in patients with UCEC (in eng). *Mol Ther Nucleic Acids*, 27: 1036–1055.

    https://doi.org/10.1016/j.omtn.2022.01.018

24. Ping L, Zhang K, Ou X, *et al.*, 2021, A novel pyroptosis-associated long non-coding RNA signature predicts prognosis and tumor immune microenvironment of patients with breast cancer (in eng). *Front Cell Dev Biol*, 9: 727183.

    https://doi.org/10.3389/fcell.2021.727183

25. Guo M, Xiao ZD, Dai Z, *et al.*, 2020, The landscape of long noncoding RNA-involved and tumor-specific fusions across various cancers (in eng). *Nucleic Acids Res*, 48(22): 12618–12631.

    https://doi.org/10.1093/nar/gkaa1119

26. Lu Z, Tang F, Li Z, *et al.*, 2022, Prognosis risk model based on pyroptosis-related lncRNAs for bladder cancer (in eng). *Dis Markers*, 2022: 7931393.

    https://doi.org/10.1155/2022/7931393

27. Aran D, Sirota M, Butte AJ, 2015, Systematic pan-cancer analysis of tumour purity (in eng). *Nat Commun*, 6: 8971.

    https://doi.org/10.1038/ncomms9971

28. Abril-Rodriguez G, RibasA, 2017, SnapShot: Immune checkpoint inhibitors (in eng). *Cancer Cell*, 31(6): 848–848.e1.

https://doi.org/10.1016/j.ccell.2017.05.010

29. Vago L, Gojo I, 2020, Immune escape and immunotherapy of acute myeloid leukemia (in eng). *J Clin Invest*, 130(4): 1552–1564.

https://doi.org/10.1172/jci129204

30. Jiang F, Wang XY, WangMY, *et al*., 2021, An immune checkpoint-related gene signature for predicting survival of pediatric acute myeloid leukemia (in eng). *J Oncol*, 2021: 5550116.

https://doi.org/10.1155/2021/55501106

31. He R, Wu S, Gao R, *et al*., 2021, Identification of a long noncoding RNA TRAF3IP2-AS1 as key regulator of IL-17 signaling through the SRSF10-IRF1-Act1 axis in autoimmune diseases (in eng). *J Immunol*, 206(10): 2353–2365.

https://doi.org/10.4049/jimmunol.2001223

32. Han Y, Ye A, Bi L, *et al*., 2014, Th17 cells and interleukin-17 increase with poor prognosis in patients with acute myeloid leukemia (in eng). *Cancer Sci*, 105(8): 933–942.

https://doi.org/10.1111/cas.12459

33. Wróbel T, Mazur G, Jazwiec B, *et al*., 2003, Interleukin-17 in acute myeloid leukemia (in eng). *J Cell Mol Med*, 7(4): 472–474.

https://doi.org/10.1111/j.1582-4934.2003.tb00250.x

34. Li J, Zhang J, Tao S, *et al*., 2022, Prognostication of pancreatic cancer using the cancer genome atlas based ferroptosis-related long non-coding RNAs (in eng). *Front Genet*, 13: 838021.

https://doi.org/10.3389/fgene.2022.838021

35. Zhong F, Yao F, Cheng Y, *et al*., 2022, m6A-related lncRNAs predict prognosis and indicate immune microenvironment in acute myeloid leukemia (in eng). *Sci Rep*, 12(1): 1759.

https://doi.org/10.1038/s41598-022-05797-5

36. Ni W, Mo H, Liu Y, *et al*., 2021, Targeting cholesterol biosynthesis promotes anti-tumor immunity by inhibiting long noncoding RNA SNHG29-mediated YAP activation (in eng). *Mol Ther*, 29(10): 2995–3010.

https://doi.org/10.1016/j.ymthe.2021.05.012

37. Chen C, Liang C, Wang S, *et al*., 2020, Expression patterns of immune checkpoints in acute myeloid leukemia (in eng). *J Hematol Oncol*, 13(1): 28.

https://doi.org/10.1186/s13045-020-00853-x

38. Han L, Li Z, Jiang Y, *et al*., 2019, SNHG29 regulates miR-223-3p/CTNND1 axis to promote glioblastoma progression via Wnt/β-catenin signaling pathway (in eng). *Cancer Cell Int*, 19: 345.

https://doi.org/10.1186/s12935-019-1057-x

39. Li S, Wu D, Jia H, *et al*., 2020, Long non-coding RNA LRRC75A-AS1 facilitates triple negative breast cancer cell proliferation and invasion via functioning as a ceRNA to modulate BAALC (in eng). *Cell Death Dis*, 11(8): 643.

https://doi.org/10.1038/s41419-020-02821-2

40. Wu L, Liao W, Wang X, *et al*., 2021, Expression, prognosis value, and immune infiltration of lncRNA ASB16-AS1 identified by pan-cancer analysis (in eng). *Bioengineered*, 12(2): 10302–10318.

https://doi.org/10.1080/21655979.2021.1996054

41. Bosman MC, Schepers H, Jaques J, *et al*., 2014, The TAK1-NF-κB axis as a therapeutic target for AML (in eng). *Blood*, 124(20): 3130–3140.

https://doi.org/10.1182/blood-2014-04-569780

42. Fu T, Ji K, Jin L, *et al*., 2021, ASB16-AS1 up-regulated and phosphorylated TRIM37 to activate NF-κB pathway and promote proliferation, stemness, and cisplatin resistance of gastric cancer (in eng). *Gastric Cancer*, 24(1): 45–59.

https://doi.org/10.1007/s10120-020-01096-y

43. Zhou JG, Liang B, Liu JG, *et al*., 2021, Identification of 15 lncRNAs signature for predicting survival benefit of advanced melanoma patients treated with Anti-PD-1 monotherapy (in eng). *Cells*, 10(5): 977.

https://doi.org/10.3390/cells10050977

44. Rezaei M, Tan J, Zeng C, *et al*., 2021, TIM-3 in leukemia; Immune response and beyond (in eng). *Front Oncol*, 11: 753677.

https://doi.org/10.3389/fonc.2021.753677

45. Kikushige Y, Akashi K, 2012, TIM-3 as a therapeutic target for malignant stem cells in acute myelogenous leukemia (in eng). *Ann N Y Acad Sci*, 1266: 118–123.

https://doi.org/10.1111/j.1749-6632.2012.06550.x

46. Du T, Gao J, Li P, *et al*., 2021, Pyroptosis, metabolism, and tumor immune microenvironment (in eng) *Clin Transl Med*, 11(8): e492.

https://doi.org/10.1002/ctm2.492

47. Park EG, Pyo SJ, Cui Y, *et al*., 2022, Tumor immune microenvironment lncRNAs (in eng). *Brief Bioinform*, 23(1): bbab504.

https://doi.org/10.1093/bib/bbab504